Desalination and Water Treatment
www.deswater.com
doi: 10.5004/dwt.2020.25729

192 (2020) 155–165
July

In-situ enhanced heavy metal ion removal efficiency based on branched amino groups in the forward osmosis process

Chaojie Cai, Xiaobin Lei, Xinzhen Zhao, Lin Wang, Jizhen Jia, Changkun Liu*

College of Chemistry and Environmental Engineering, Shenzhen University, Shenzhen, 518060, Guangdong Prov, China, emails: liuck@szu.edu.cn (C. Liu), 1804121659@qq.com (C. Cai), 826798147@qq.com (X. Lei), mrxinzhen@163.com (X. Zhao), 782792504@qq.com (L. Wang), 1195866282@qq.com (J. Jia)

Received 30 August 2019; Accepted 18 February 2020

ABSTRACT

Modification of the active layer is an effective method to improve the separation performance of the thin-film composite forward osmosis (FO) membranes. In this paper, the dendrimer polyamidoamine (PAMAM) was in-situ integrated into the polyamide (PA) active layer via the interfacial polymerization. The separation performance results showed that the addition of PAMAM significantly improved the separation water flux of the modified FO membrane by 1.7 times, and the reverse salt flux was almost unchanged. In addition, the removal efficiency of the modified FO membrane for heavy metal ions was enhanced, with the rejection rates of various heavy metal ions all higher than 99.6%, and the corresponding water flux was also significantly enhanced. The PAMAM integrated with the active layer contained a large number of hydrophilic segments and terminal amine groups, which in situ enhanced the hydrophilicity and permeability of the active layer, and further improved the removal of heavy metal ions based on the coordination and electrostatic repulsion effects. The purpose of this paper is to provide a feasible way to improve the practical application performance of the FO membranes.

Keywords: Forward osmosis; Polyamidoamine; Heavy metal ions; Separation efficiency

1. Introduction

Heavy metals in the ecological environment as non-degradable pollutants can access the human body via the food chain and damage the central nervous system and organs. The pollution of water by heavy metal ions has been a serious threat to human health and ecological security [1–3]. Therefore, heavy metal ions in water need to be removed by various effective techniques, such as chemical precipitation, adsorption, membrane separation technology, etc [4–7]. It is noteworthy that the forward osmosis (FO) separation technology is suitable for heavy metal wastewater treatment based on the unique advantages, such as low membrane pollution and low energy consumption [8–11]. However, based on the current development of the FO technology, it is imperative to prepare FO membranes with high separation efficiency.

The separation performance of the FO membrane is directly determined by the characteristics of the active layer in actual separation processes. It is known that the active layer of the FO membrane is the area where the solute and solvent are separated due to the effect of the osmotic pressure. Current research work aims to improve the permeability and rejection ability of the active layer simultaneously. The purpose of the modification for the active layer such as blending and surface grafting is to change the physical and chemical properties of the active layer matrix. The surface grafting methods generally include the surface-initiated graft polymerization or the reaction with terminal functional groups to fix the functional polymers

* Corresponding author.

on the active layer for the enhancement of the functionalities such as hydrophilicity, retention, fouling resistance and antibacterial properties [12–17]. However, the means of surface grafting may not be suitable for large-scale implementation due to the rigorous experimental operation processes. In contrast, the blending method is simple and easy to operate, and the functional nanoparticles or polymers can be added in the water phase or organic phase to change the physicochemical properties of the PA layer, thus improving the desalination, salt-resistance and antifouling properties. Most of the blending methods show the advantages of hybrid modification to introduce the functionalities to the active layer and improve the separation efficiency of the FO membranes [18–20].

The modification of the active layer needs to take both the permeability and the rejection into consideration. In the case of the aquaporin-modified active layer, the aquaporin not only provides penetration channels for water molecules but also precisely rejects ions through the charge characteristics of its internal channels. Due to the dual functions, aquaporins have both high water permeability and excellent ion rejection ability. Therefore, the modifier for the active layer needs to have unique multiple functions [21–25]. As we all know, dendrimers are a kind of practical and functional polymers with a large number of functional groups and molecular chains, which are beneficial to giving full play to its special functions. Polyamidoamine (PAMAM) is a commonly-used functional dendrimer with a hyperbranch structure, abundant terminal amine groups, and a nearly spherical molecular structure [26–28]. If PAMAM is used to modify the PA active layer, the branched structure, intramolecular cavity, and the nearly spherical nanostructure of PAMAM are able to increase the free volume, enhance the hydrophilicity and reduce the mass transfer resistance of the densely-crosslinked PA active layer. In addition, the PAMAM molecules have a large number of hydrophilic amine groups which can enhance the hydrophilicity and the ability to adsorb heavy metal ions of the active layer.

In this paper, the dendrimer PAMAM as a functional modifier was added into the PA active layer to prepare thin-film composite (TFC)-type FO membranes through the interfacial polymerization reaction. The physicochemical properties of this TFC-type FO membrane before and after the PAMAM modification were characterized, and the separation performance of the FO membrane for heavy metal ions in wastewater was studied. The aim of this paper is to reveal the effect of the functional modifier PAMAM on the removal mechanism of heavy metal ions in the FO process.

2. Experimental

2.1. Materials

Polyvinylidene fluoride (PVDF, 0.22 μm) flat membranes were purchased from Taoyuan Chemical Co. Ltd., (Haining, China). Polyamidoamine (PAMAM, Generation 2, M_w = 3,256 g mol^{-1}) dendrimer was purchased from CY Dendrimer Technology Co. Ltd., (Weihai, China). Copper sulfate ($CuSO_4$), zinc nitrate ($Zn(NO_3)_2$), nickel nitrate ($Ni(NO_3)_2$), lead nitrate ($Pb(NO_3)_2$), cadmium nitrate ($Cd(NO_3)_2$), m-Phenylenediamine (MPD, 99%) and trimesoyl chloride (TMC, 97%) were all purchased from Aladdin, China. Magnesium chloride hexahydrate ($MgCl_2{\cdot}6H_2O$, AR, 98%), acrylic acid (AA, AR, >99%) were purchased from Macklin Reagent Co. Ltd., China. The deionized (DI) water was prepared from the ultrapure water system (ULUPURE, China).

2.2. Preparation of the TFC-type FO membranes

The active layer of the TFC-type FO membrane was prepared via the interfacial polymerization method on PVDF membrane substrates. During the whole process, the PVDF membrane substrate was fixed in the lab-made experimental device with only the upper surface allowed for the interfacial polymerization. The interfacial polymerization reaction with MPD and TMC was carried out to produce the active layer of the conventional FO membrane. The upper surface of the PVDF membrane was first completely immersed in 2 wt.% MPD/water solution for 2 min. After that, the residue solution was removed with a filter paper. Then, the as-prepared upper surface of the PVDF membrane substrate was further immersed in 0.2 wt.% TMC/*n*-hexane solution for 1 min before the solution was removed. The freshly prepared TFC-type FO membrane was dried in an oven at 80°C for 5 min, stored in DI water for further use, and named as M-0. The PAMAM-modified TFC-type FO membrane was prepared via the interfacial polymerization reaction with the PAMAM/MPD mixture in the water phase and TMC in the *n*-hexane phase. The interfacial polymerization reaction mechanism with PAMAM, MPD, and TMC is shown in Fig. 1. The PAMAM/MPD mixture with four different PAMAM concentrations (0.1, 0.2, 0.3, and 0.4 wt./v%) was prepared by mixing different amounts of PAMAM with 2 wt.% MPD water solutions, and the prepared membrane was marked as M-1, M-2, M-3, and M-4, respectively. M-5 membrane was also prepared via the same interfacial polymerization with 1.0 wt.% PAMAM/water solution and 0.2 wt.% TMC/*n*-hexane solution as the reactants, without the addition of MPD.

2.3. Characterization of the prepared TFC-type FO membranes

The attenuated total reflectance Fourier transform infrared spectroscopy (ATR-FTIR, Bruker V70, Germany) was used to test the surface functional groups of the prepared membranes, with the scanning wavenumber range of 600–4,000 cm^{-1} and a resolution of 4 cm^{-1}. The X-ray photoelectron spectrometer (XPS, Thermo Fisher Scientific ESCALAB 250Xi, USA) was used to analyze the surface element information of the prepared membranes. The field emission scanning electron microscope (Shimadzu JSM-7800F, Japan) was used to characterize the surface morphology of the prepared FO membranes. The water contact angle (WCA) measuring system (SDC-70, Shengding, China) was used to investigate the surface hydrophilicity of the prepared membranes. The WCA measurement was carried out at 3 randomly-chosen places of the membrane surface and an average value was used for the hydrophilicity analysis.

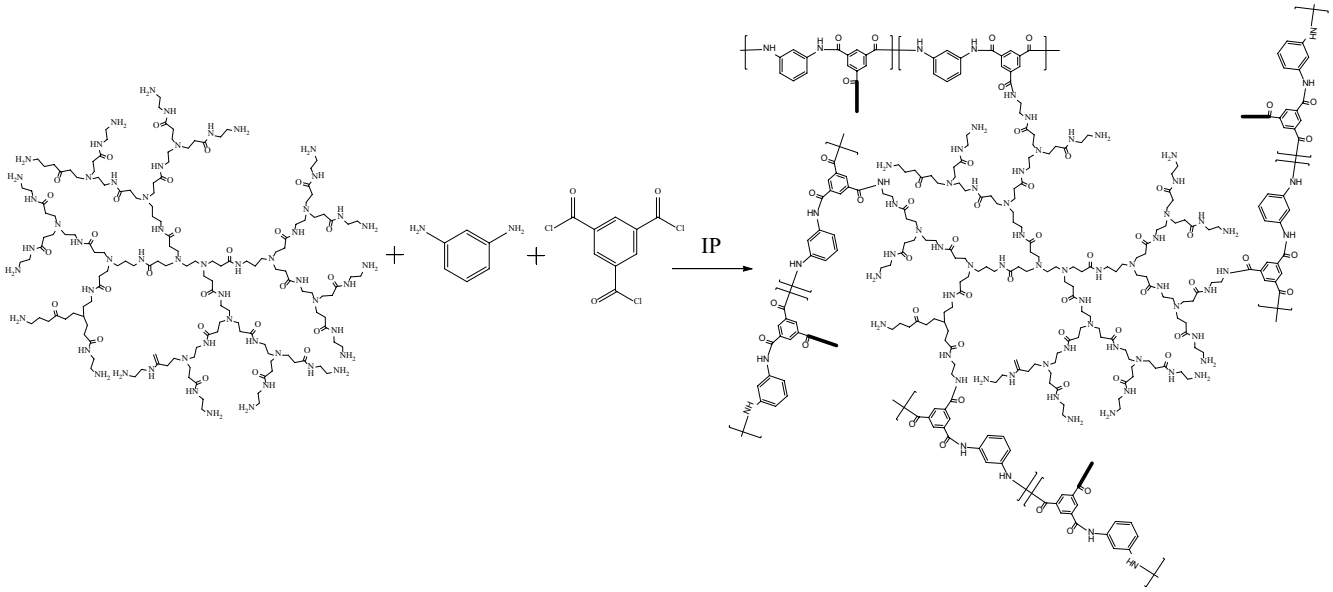

Fig. 1. Possible molecular structures formed from the interfacial polymerization reaction of PAMAM, MPD, and TMC.

2.4. FO performance evaluation of the prepared TFC-type FO membranes

The water permeability coefficient (A, L m^{-2} h^{-1} bar^{-1}, abbreviated as LMH bar^{-1}) and the salt permeability coefficient (B, L m^{-2} h^{-1}, abbreviated as LMH) of the prepared FO membranes were determined in a reverse osmosis unit with the dead-end filtration, which was pre-compacted for 0.5 h under the pressure of 1 bar using DI water and 10 mM $MgCl_2$ as feed solutions. A and B values were calculated from Eqs. (1)–(3).

$$A = \frac{\Delta Q}{A_m \Delta P} \tag{1}$$

$$\frac{1 - R_s}{R_s} = \frac{B}{A\left(\Delta P - \Delta\pi\right)} \tag{2}$$

$$R_s = \left(1 - \frac{\Lambda_p}{\Lambda_f}\right) \times 100\% \tag{3}$$

where A_m (m^2) is the active area of the membrane (9 cm^2), ΔQ (L/h) denotes the penetrated volume flow of the pure water within the penetrating time (t), ΔP (bar) denotes the applied pressure difference, $\Delta\pi$ (bar) denotes the osmotic pressure difference across the membrane, and R_s (%) is the salt rejection which is determined by the conductivity of the penetrating fluid (Λ_p) and the feed solution (10 mM $MgCl_2$) (Λ_f) using a conductivity meter (Rex Electric Chemical DDS-307A).

The pure water flux (J_w, L m^{-2} h^{-1}, abbreviated as LMH) and the reverse salt flux (J_s, g m^{-2} h^{-1}, abbreviated as gMH) of the prepared FO membranes were determined using the lab-made FO testing device. DI water and $MgCl_2$ solution were used as feed solution and draw solution, respectively. The increase of the draw solution volume was monitored, and the salt concentration changes in the feed solution were tested using the conductivity meter. The calculation of J_w and J_s are shown in Eqs. (4) and (5).

$$J_w = \frac{\Delta V}{A_m \Delta t} \tag{4}$$

$$J_s = \frac{C_{f,t} V_{f,t} - C_{f,i} V_{f,i}}{A_m \Delta t} \tag{5}$$

where ΔV (L) is the draw solution volume increase at the permeation time Δt (h), A_m (m^2) is the area of the membrane (9 cm^2), $V_{f,i}$ and $V_{f,t}$ (L) are the feed solution volume before and after the FO test, respectively, and $C_{f,i}$ and $C_{f,t}$ (mol L^{-1}) are the salt ($MgCl_2$) concentrations in the feed solution before and after the FO test, respectively.

For the investigation of the heavy metal ion removal performances, five kinds of heavy metal ions (Cu^{2+}, Ni^{2+}, Pb^{2+}, Zn^{2+}, and Cd^{2+} ions) were separately prepared as feed solutions with concentrations of 1, 2, and 5 g/L, respectively. The pH values were adjusted in the range of 1–4 for the study of the pH effect on the FO performance. The heavy metal ion rejection R_h (%) was defined as the percentage of the rejected heavy metal ions in the feed solution during the FO process, as determined in Eq. (6).

$$R_h = \left(1 - \frac{C_d V_d}{C_f V_p}\right) \times 100\% \tag{6}$$

where C_d (g/L) and V_d (L) are the heavy metal ion concentration in the draw solution and the draw solution volume, respectively, after the FO process. V_p (L) is the total volume of the permeated water, and C_f (g/L) is the heavy metal ion concentration in the feed solution. C_d (g/L) and C_f (g/L) were

determined by inductively coupled plasma optical emission spectrometry (ICP-OES, OPTIMA2100DV).

The actual concentration of the heavy metal ions ($C_{s(t)}$) in the draw solution can be calculated according to Eq. (7).

$$C_{s(t)} = \frac{C_{ds(t)}V_{ds(t)} - C_{ds(t-1)}V_{ds(t-1)}}{V_{w(t)}} \quad (7)$$

where $C_{ds(t)}$ and $C_{ds(t-1)}$ are the concentration of heavy metal ions in the draw solution (mol L^{-1}) at the pre-determined time (t) and the previous predetermined time (t–1), respectively. $V_{ds(t)}$ and $V_{ds(t-1)}$ are the volume of the draw solution (L) at a time (t) and time (t–1), respectively. $V_{w(t)}$ is the penetrated pure water volume (L) at a time (t).

3. Results and discussion

3.1. Characterization of the prepared FO membranes

The FO membranes were prepared by means of interfacial polymerization on top of the PVDF supporting layer to fix the functional skin layer. Fig. 2 shows the ATR-FTIR spectra for the top surface of the PVDF and the prepared FO membranes. It could be seen that new peaks appeared at 1,654, 1,610 and 1,544 cm^{-1} for M-0 as compared with the PVDF membrane, which belonged to the carbonyl stretching vibration (amide I), aromatic amine and amide N–H bending vibration (amide II) [29–31]. The characteristic peaks at 1,654 and 1,544 cm^{-1} slightly increased with the increase of the PAMAM addition in the PA layer. These results indicated that PAMAM containing a large amount of amine and amide groups was anchored in the active layer of the FO membrane though the interfacial crosslinking.

Fig. 3 shows the XPS spectra of the PVDF and the prepared FO membranes. The surface of the prepared membranes consisted of carbon (C), oxygen (O), nitrogen (N), and fluorine (F) elements, and the atomic percentage of each element is shown in Table 1. The F content shows a sharp decrease while the O and N atomic percentage increased for the prepared FO membranes (M-n, n = 0–5) as compared with the PVDF membrane, indicating the successful coverage of the PA layer via the interfacial polymerization on the PVDF membrane surface. Compared with M-0, the N atomic percentage of M-n (n = 1–5) increased as the addition of PAMAM increased, which was attributed to the high N contents in PAMAM molecules. The result showed that the PAMAM was anchored in the PA layer which changed the surface chemical properties of the prepared FO membranes.

Fig. 4 shows the top surface morphologies of the PVDF and the prepared FO membranes. The PVDF membrane showed conventional porous structures, and M-0 membrane exhibited the typical "peak-valley" structures on the membrane surface, which was the characteristic morphology of the PA active layer [32,33]. However, the PAMAM-modified FO membranes (M-1, M-2, M-3, and M-4) showed less "peak-valley" structures with reduced roughness, which was probably due to the addition of PAMAM which changed the original cross-linking mode of MPD and TMC. It was especially noted for M-5 that the particle-like morphology

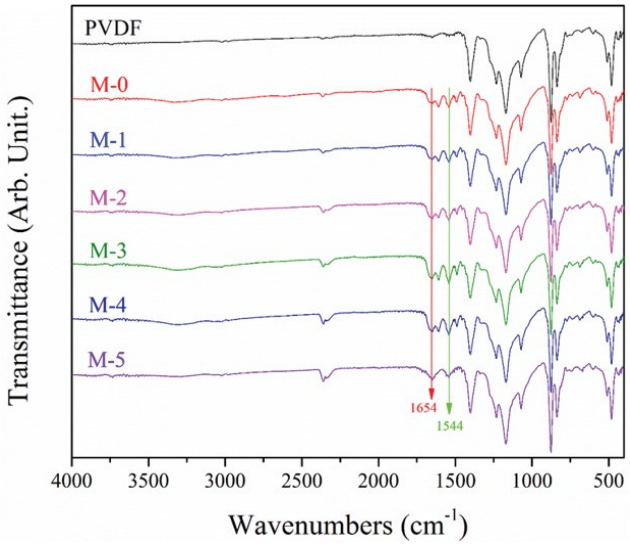

Fig. 2. ATR-FTIR spectra of PVDF and M-n membranes.

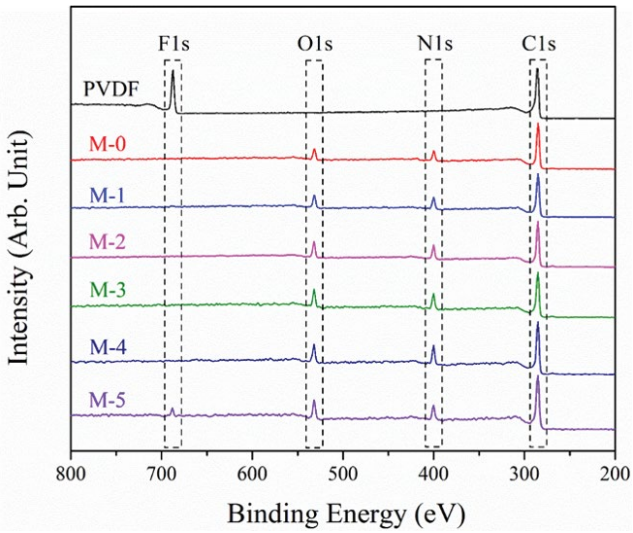

Fig. 3. XPS spectra of PVDF and M-n membranes.

Table 1
Detailed surface element compositions (atomic %) of the prepared membrane surfaces derived from the XPS characterization results

Membranes	Element content (at %)			
	C (%)	F (%)	O (%)	N (%)
PVDF	80.15	18.87	0.99	0
M-0	78.13	0.81	8.41	12.65
M-1	75.59	0.76	9.96	13.70
M-2	74.56	0.14	10.86	14.44
M-3	72.79	0.80	11.02	15.40
M-4	73.22	0.79	9.94	16.05
M-5	75.43	3.56	10.05	10.97

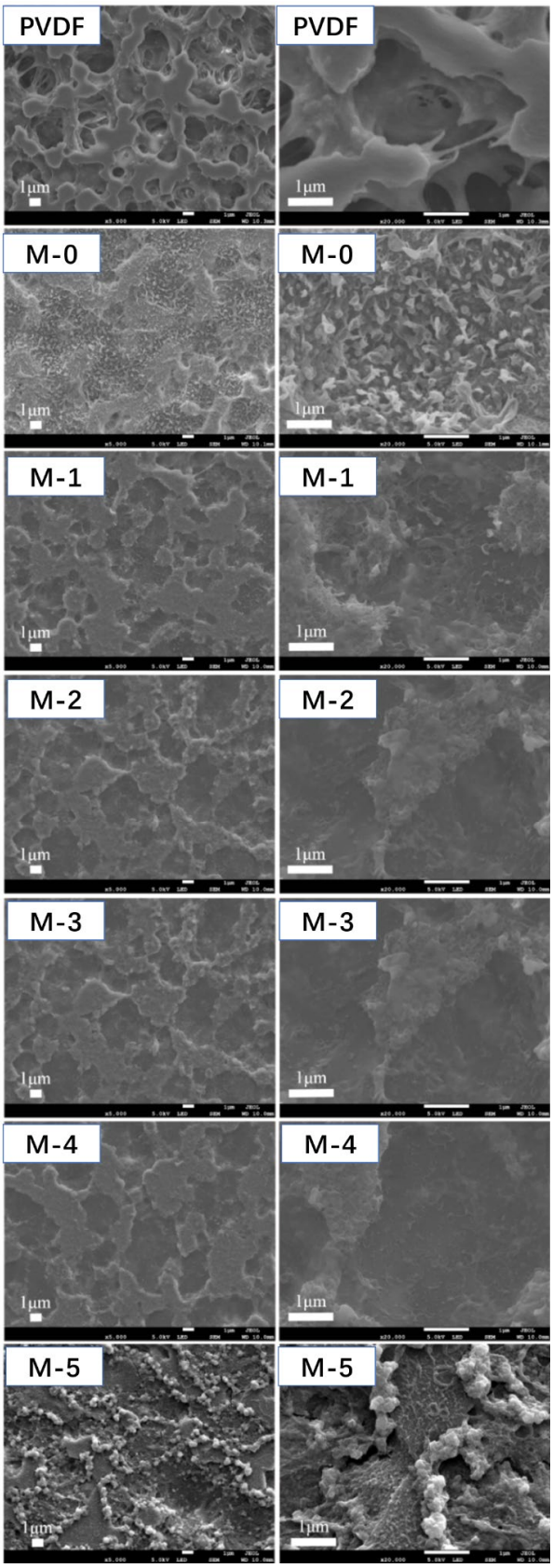

Fig. 4. FESEM images of PVDF and the prepared FO membranes surface.

instead of the "peak-valley" structures prevailed on the top surface, which could be attributed to the geometric size of the PAMAM. These FESEM observations showed the obvious changes for the top surface morphologies of the PAMAM-modified FO membranes.

The water contact angle (WCA) of the PVDF and the prepared FO membranes is shown in Fig. 5. The PVDF membrane was hydrophobic with the surface WCA value of 124°. For M-0, the WCA decreased to 76.5° due to the coverage of the PA active layer. The WCA showed a further steady decrease for M-1 to M-5 membranes due to the increasing amount of the PAMAM molecules containing a large number of hydrophilic amine groups which improved the wettability of the PA layer.

3.2. FO performance

The FO performance of the modified FO membranes including the pure water flux and the reverse salt flux is shown in Fig. 6. M-2 shows the highest water flux in both AL-FS and AL-DS modes. The water flux of M-2 was 1.7 and 1.6 times that of the M-0 in AL-DS and AL-FS mode, respectively. The reverse salt flux showed a slightly increasing trend based on the increased amount of PAMAM in the active layer. The separation selectivity (J_w/J_s) of the M-2 membrane also significantly improved based on the significantly increased water flux and the stable reverse salt flux. As the PAMAM molecules owned the nearly spherical nanostructure and the amine groups, the proper amount of PAMAM polymerized in the PA layer would relatively increase the free volume and the hydrophilicity of the PA layer, hence reducing the permeation resistance of the water molecules across the membranes [34]. However, the larger amount of PAMAM polymerized in the PA layer would introduce more spherical nanostructures and free space, which was also beneficial for the reverse osmosis of salt ions.

In order to distinguish the impact of the added PAMAM quantity on the membrane permeability, *A*, *B*, and *B*/*A*

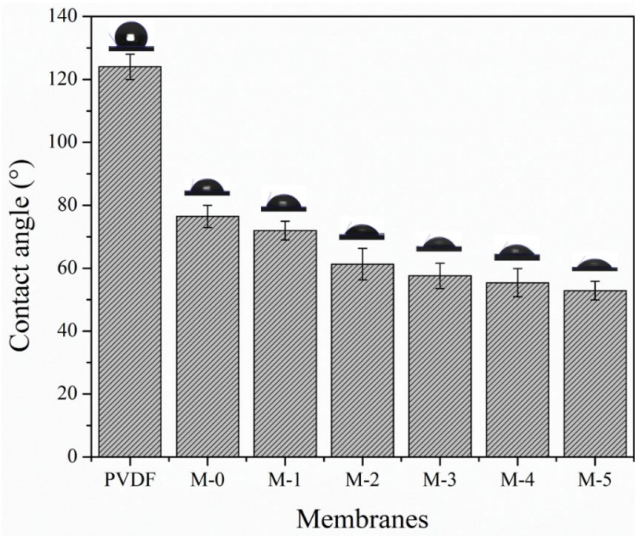

Fig. 5. Water contact angles of PVDF and the prepared FO membranes.

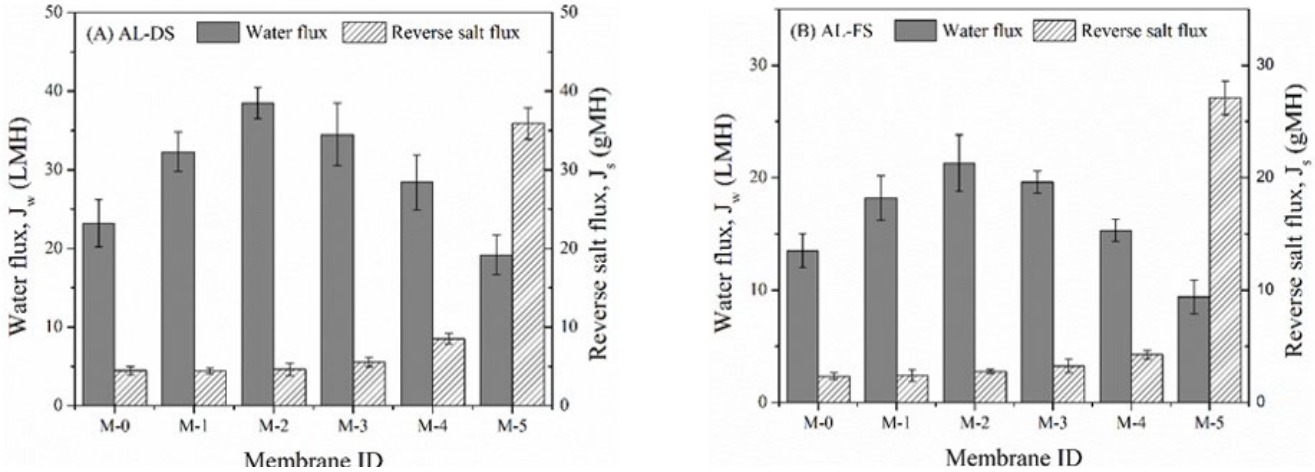

Fig. 6. Water flux and reverse salt flux of the M-*n* membranes. Draw solution: 2 M $MgCl_2$; feed solution: DI water; at room temperature.

values of the TFC-type FO membranes were investigated. The *B*/*A* value was a critical parameter in assessing the membrane selectivity. The smaller the *B*/*A* value, the better the FO membrane selectivity. As shown in Table 2, the *A*, *B*, and *B*/*A* values of the TFC-type FO membranes gradually increased as the increase of the added PAMAM amount. The *B*/*A* value of M-2 was relatively similar to M-0, while the *B*/*A* value of M-5 was the highest, indicating that M-2 showed much better membrane selectivity than M-5 and that the appropriate amount of PAMAM in the active layer was conducive to improving the separation performance of the TFC-type FO membranes. Therefore, the results indicated that the proper amount of PAMAM addition in the PA layer was helpful to improve the pure water flux and selectivity of the TFC-type FO membranes, and the M-2 membrane was selected for further investigations.

Test conditions: testing pressure of 1.0 bar, DI water, and 10 mM $MgCl_2$ as feed solutions, at the room temperature of 25°C. Error estimation was based on the standard deviation of 3 independent sample measurements.

3.3. Study on the performance of the TFC-type FO membrane in removing heavy metal ions

The separation performance of M-2 and M-0 membrane in removing heavy metal ions are shown in Fig. 7. For the feed solutions of several metal ions, the pure water flux of M-2 membrane was about 35 and 18.5 LMH in AL-DS and AL-FS modes, respectively. These values were significantly higher than those of M-0. Figs. 7b and d show that M-2 and M-0 membrane had similar rejection of the five heavy metal ions, with the rejection of Ni^{2+}, Cu^{2+}, Pb^{2+}, Zn^{2+}, and Cd^{2+} ions to be 99.6%, 99.9%, 99.7%, 99.8%, and 99.8%, respectively. The results demonstrated that PAMAM could significantly improve the pure water flux and ensure the selectivity of the FO membranes. PAMAM molecules owned the nano-size morphology and plenty of terminal amine groups that could increase the free volume and hydrophilicity of the PA layer which in turn reduced the permeation resistance of the water molecules [35,36]. In addition, the complexing effect between the terminal amine groups in PAMAM in the PA layer and the heavy metal ions were significantly enhanced which resulted in the high rejection ability of the heavy metal ions in solution by the adsorbed heavy metal ions via the electrostatic repulsive force.

Fig. 8 shows the effect of operating time on the pure water flux and heavy metal ion rejection of M-0 and M-2 membranes during the FO process. The pure water flux of M-2 membrane slightly decreased from 19.0 to 17.1 LMH after 360 min, dropping by 10.0%. As compared, the pure water flux of M-0 membrane decreased from 12.0 LMH to 8.2 LMH after 360 min, with a decreasing ratio of 31.7%.

Table 2
Characteristics of the TFC-type FO membranes

Membranes	Water permeability, A (LMH bar^{-1})	Salt rejection, R_s (%)	Salt permeability, B (LMH)	B/A (kPa)
M-0	2.34 ± 0.21	97.4 ± 1.1	0.06 ± 0.02	2.7 ± 1.2
M-1	2.52 ± 0.30	97.0 ± 1.5	0.08 ± 0.04	3.1 ± 1.6
M-2	2.63 ± 0.15	96.8 ± 1.0	0.09 ± 0.03	3.3 ± 1.1
M-3	2.70 ± 0.42	96.2 ± 1.4	0.11 ± 0.03	4.0 ± 1.5
M-4	2.85 ± 0.20	95.6 ± 0.8	0.13 ± 0.02	4.6 ± 0.9
M-5	3.21 ± 0.35	83.5 ± 1.8	0.63 ± 0.02	19.8 ± 2.6

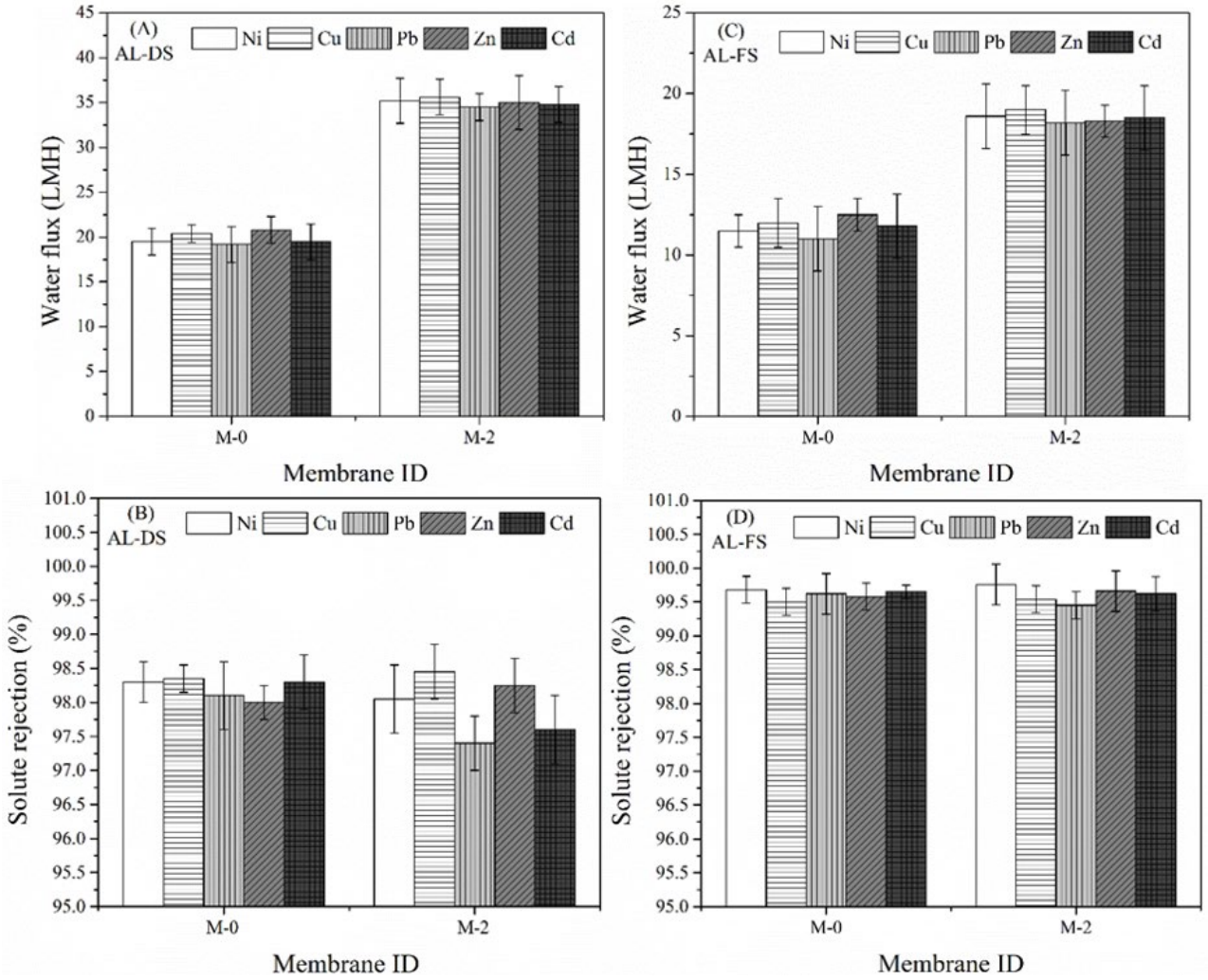

Fig. 7. Water flux (a–c) and solute rejection (b–d) of the M-0 and M-2 membranes. Draw solution: 2 M $MgCl_2$; feed solution: 2 g/L; pH = 4; at room temperature.

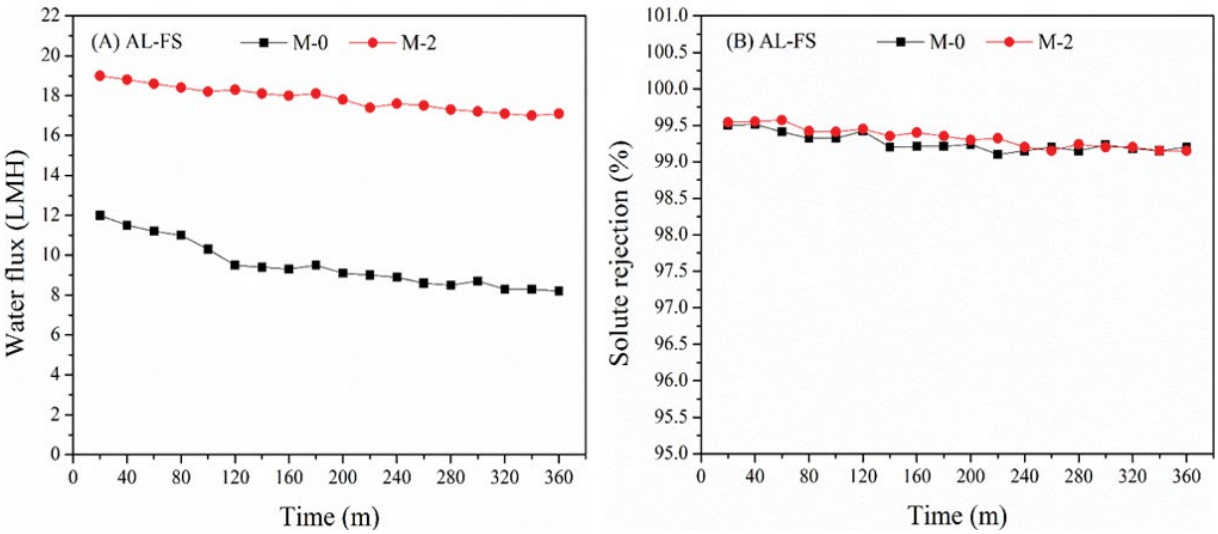

Fig. 8. (a) Water flux and (b) solute rejection of the M-0 and M-2 membranes as the function of the time draw solution: 2 M $MgCl_2$; feed solution: 2 g/L Cu^{2+}; pH = 4; at room temperature.

The rejection of heavy metal ions of the two membranes was basically identical as the rejections were still above 99.2% at 360 min. It shows that the modified FO membranes were stable in the removal performance for heavy metal ions during the FO process.

Fig. 9 shows the effect of temperature and pH on the pure water flux and the heavy metal ion rejection of the M-2 membrane. When the temperature increased from 25°C to 65°C, the pure water flux increased from 18.6 LMH to 24.0 LMH (Fig. 9a), increasing by 29.0%. As the osmotic pressure of the solution was directly proportional to the temperature, the increase of the driving force at both sides of the membrane led to the increase of the pure water flux. It is from Fig. 9b that the rejection of heavy metal ions slightly decreased as the temperature increased, possibly due to the acceleration of the diffusion speed as a result of the increase of the temperature and the pure water flux, thereby decreasing the rejection of heavy metal ions. However, the rejection of heavy metal ions was still higher than 99.3% at 65°C. Figs. 9c and d show the impact of pH on the pure water flux of M-0 and M-2 membranes, which was relatively insignificant as the pure water flux basically remained the same. The rejection of heavy metal ions slightly decreased with the decrease of the pH of the feed solution. Therefore, the separation performance of M-0 and M-2 membranes was stable in the acidic separation environment.

It is from Fig.10a that the feed solution concentration increased from 1 to 5 g/L and the pure water flux of M-2 decreased from 20.2 to 16.4 LMH. The pure water flux reduced due to the decrease of the osmotic pressure difference with the increase of the feed solution concentrations. When the feed solution concentration was 1 g/L, the rejection of heavy metal ions was about 99.7%. When the feed solution concentration increased to 2 g/L, or even to 5 g/L, the rejections of heavy metal ions were still higher than 99.4% (Fig. 10b). When the draw solution concentration increased from 0.5 to 2 M, the pure water flux under AL-FS mode increased from 9.0 to 18.5 LMH, and the increasing rate of the pure water flux was only 105.6% (Fig. 10c). The increasing rate of the pure water flux was not directly proportional

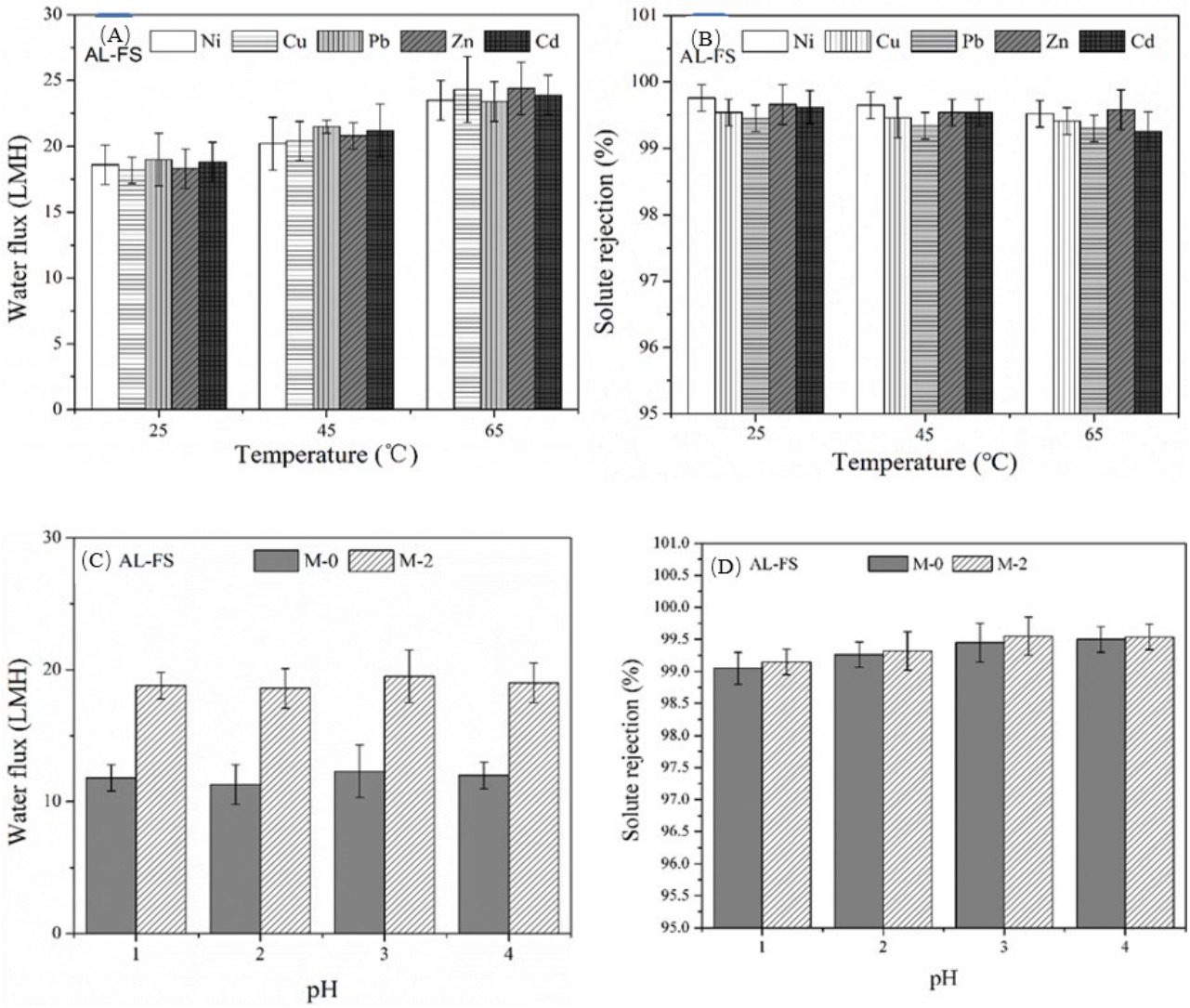

Fig. 9. Effect of temperature and pH on the separation performance of M-2 membrane (draw solution: 2 M $MgCl_2$; feed solution: 2 g/L).

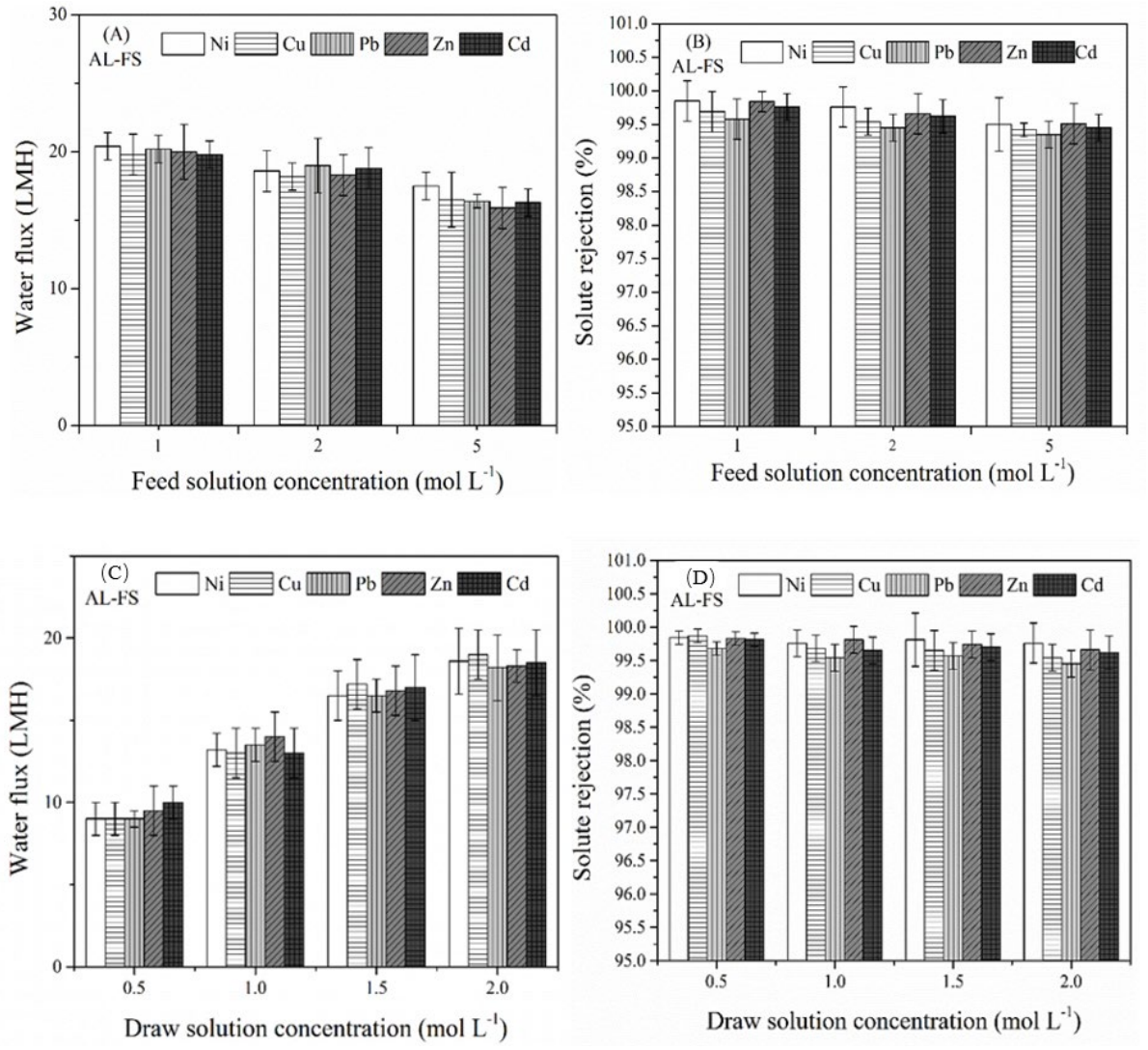

Fig. 10. (a) Water flux, (b) solute rejection of the M-2 membrane as the function of the feed solution concentration. Draw solution: 2 M $MgCl_2$, (c) Water flux, and (d) solute rejection of the M-2 membrane as a function of the draw solution concentration. Feed solution: 2 g/L; pH = 4; at room temperature.

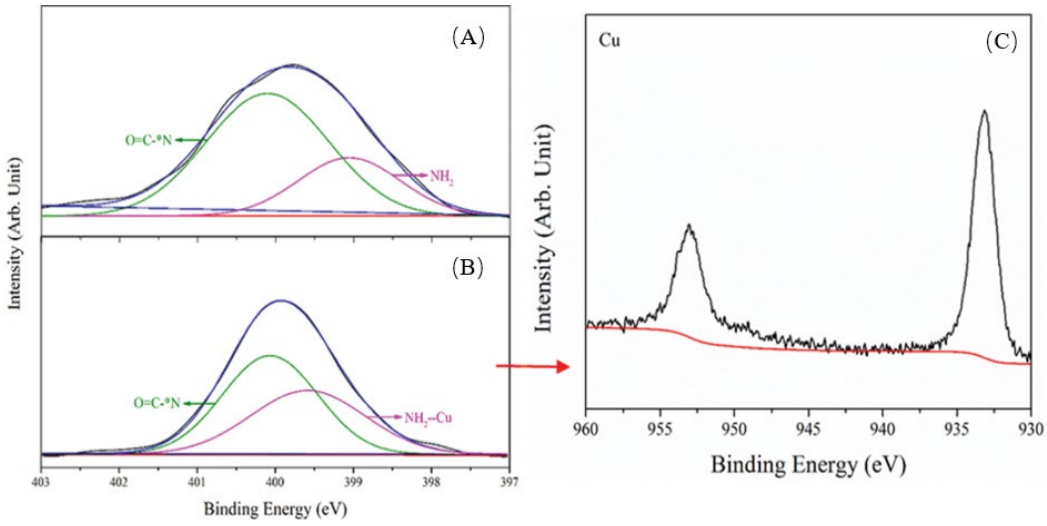

Fig. 11. XPS N 1s spectra of (a) M-2, (b) M-2-Cu membranes, and (c) Cu 4f spectra of M-2-Cu membranes.

to the increase of the draw solution concentration, which was due to the inner concentration polarization impact in the supporting layer. Fig. 10d shows that the rejection of heavy metal ions basically remained the same as the draw solution concentration increased. Theoretically, the diffusion coefficient of heavy metal ions increased as the heavy metal ion concentration increased, and the diffusion flux was in direct proportion to the ion concentrations. However, the increase of the feed solution concentration reduced the driving force on both sides of the membrane, leading to the reduction of the pure water flux. Furthermore, the branched amine groups of PAMAM in the PA layer were able to adsorb heavy metal ions through the metal-amine coordination, which would in turn enhance the positive charge of the membrane surface. Therefore, the positively-charged metal ions coordinated on the membrane surface would show the electrostatic repulsive force towards the incoming metal cations in the feed solution, and hence the rejection of metal ions would be enhanced [36–38]. As a result, the rejection of M-2 for heavy metal ions could be stable in a variety of separation environments.

3.4. Mechanism of removing heavy metal ions with M-2 membrane

The XPS characterization in Fig. 11 shows that there were two deconvoluted peaks in the N 1s core-level spectrum of M-2 at the binding energy of 399.1 and 400.1 eV, which were attributable to neutral amine (–NH_2 or >NH) and amide (O=C–N) groups, respectively. For the copper ion-adsorbed M-2 membrane during the FO process, two sub-peaks were also deconvoluted in the N 1s core-level spectrum (Fig. 11b). The peak at the binding energy of 399.7 eV was attributed to the Cu^{2+} ion-coordinated amine groups, which showed an increase as compared to that of the neutral amine groups (399.1 eV) due to the lone pair of electrons which were shared in the Cu–N coordination hybrid orbital [10]. The adsorption of Cu ions is also demonstrated in Fig. 11c which is the Cu 4f core-level spectrum detected on the Cu ion-adsorbed FO membranes. In addition, the EDX mapping images of the FO membranes with different metal ions adsorbed are shown in Fig. 12. It can be seen that Cu, Cd, Zn, Pb, and Ni ions could be adsorbed respectively on the skin layer of the prepared FO membranes due to the many-branched amine groups of PANAM present in the active layer. Therefore, the positive charge of the adsorbed metal ions on the membrane surface would show the charge repulsion effect towards the heavy metal ions in the feed solution [37–39]. As a result, the rejection of heavy metal ions was significantly improved.

4. Conclusions

The PAMAM-modified TFC-type FO membrane was prepared in this study, which could not only significantly increase the water flux of the membrane, but also efficiently remove a variety of heavy metal ions. The addition of PAMAM could improve the hydrophilicity of the active layer and reduce the permeability resistance of the water molecules through the membrane. The branched amine groups could effectively adsorb heavy metal ions, which would in turn exhibit charge repulsion effect towards the heavy metal ions in the feed solution, thus enhancing the rejection ability to the heavy metal ions. Therefore, the functional modification of the FO membrane with PAMAM in the active layer would effectively promote the application of

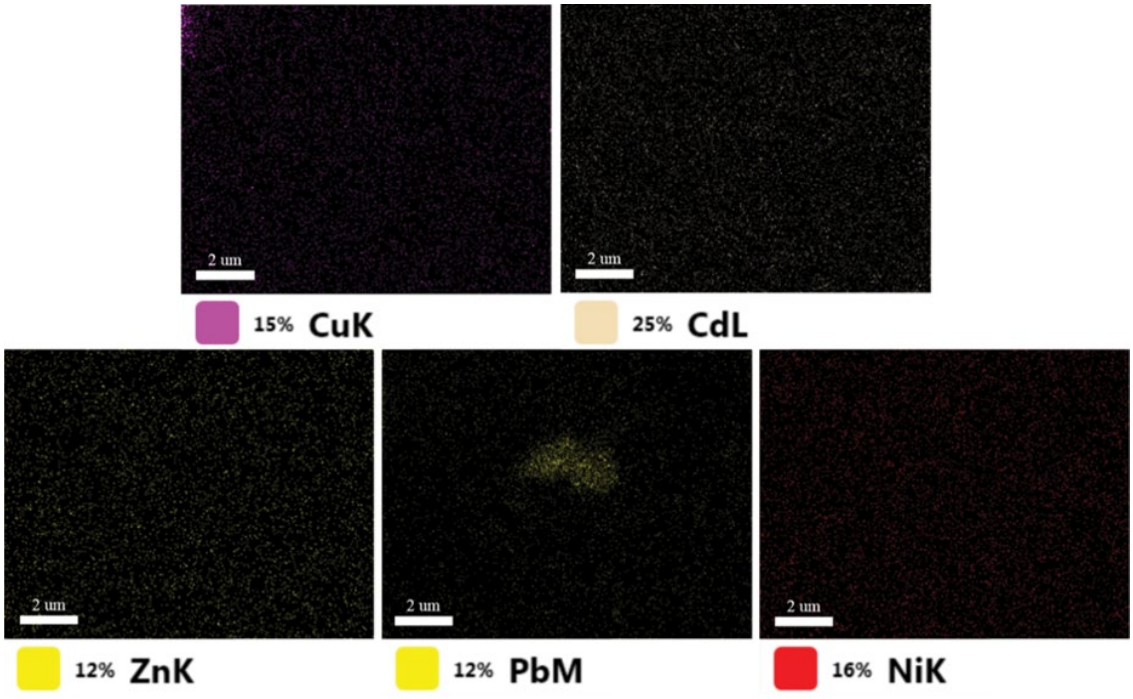

Fig. 12. EDX mapping of copper, cadmium, zinc, lead, and nickel after the FO experiments.

FO membranes in the treatment of the heavy metal wastewater during the FO process.

Acknowledgment

This work was financially supported by the National Natural Science Foundation of China (21777105), and the Shenzhen Science and Technology Foundations (JCYJ20180507182040308; JCYJ20170818101137960).

References

[1] C. Wang, W. Li, M. Guo, J. Ji, Ecological risk assessment on heavy metals in soils: use of soil diffuse reflectance mid-infrared Fourier-transform spectroscopy, Sci. Rep., 7 (2017) 40709.
[2] M. Li, H. Gou, I. Al-Ogaidi, N. Wu, Nanostructured sensors for detection of heavy metals: a review, ACS Sustainable Chem. Eng., 1 (2013) 713–723.
[3] G. Aragay, J. Pons, A. Merkoci, Recent trends in macro-, micro-, and nanomaterial-based tools and strategies for heavy-metal detection, Chem. Rev., 111 (2011) 3433–3458.
[4] Y. Yu, J.G. Shapter, R. Popelka-Filcoff, Copper removal using bio-inspired polydopamine coated natural zeolites, J. Hazard. Mater., 273 (2014) 174–182.
[5] C.V. Gherasim, J. Křivčík, P. Mikulášek, Investigation of batch electrodialysis process for removal of lead ions from aqueous solutions, Chem. Eng. J., 256 (2014) 324–334.
[6] T.A. Kurniawan, G.Y.S. Chan, W.H. Lo, S. Babel, Physico-chemical treatment techniques for wastewater laden with heavy metals, Chem. Eng. J., 118 (2006) 83–98.
[7] T. Zhou, T.T. Lim, S.S. Chin, A.G. Fane, Treatment of organics in reverse osmosis concentrate from a municipal wastewater reclamation plant: feasibility test of advanced oxidation processes with/without pretreatment, Chem. Eng. J., 166 (2011) 932–939.
[8] C.K. Liu, X.B. Lei, X.Y. Liang, J.Z. Jia, L. Wang, Visible sequestration of Cu^{2+} ions using amino-functionalized cotton fiber, RSC Adv., 7 (2017) 9744–9753.
[9] S.J. You, J.D. Lu, C.Y. Tang, X.H. Wang, Rejection of heavy metals in acidic wastewater by a novel thin-film inorganic forward osmosis membrane, Chem. Eng. J., 320 (2017) 532–538.
[10] C.K. Liu, X.B. Lei, L. Wang, J.Z. Jia, X.Y. Liang, X.Z. Zhao, H. Zhu, Investigation on the removal performances of heavy metal ions with the layer-by-layer assembled forward osmosis membranes, Chem. Eng. J., 327 (2017) 60–70.
[11] Y. Cui, Q. Ge, X.Y. Liu, T.S. Chung, Novel forward osmosis process to effectively remove heavy metal ions, J. Membr. Sci., 467 (2014) 188–194.
[12] P. Zhao, B.Y. Gao, Q.Y. Yue, S.C. Liu, H.K. Shon, The performance of forward osmosis in treating high-salinity wastewater containing heavy metal Ni^{2+}, Chem. Eng. J., 288 (2016) 569–576.
[13] R.L. McGinnis, M. Elimelech, Energy requirements of ammonia-carbon dioxide forward osmosis desalination, Desalination, 207 (2007) 370–382.
[14] B. Mi, M. Elimelech, Organic fouling of forward osmosis membranes: fouling reversibility and cleaning without chemical reagents, J. Membr. Sci., 348 (2010) 337–345.
[15] A. Achilli, T.Y. Cath, E.A. Marchand, A.E. Childress, The forward osmosis membrane bioreactor: a low fouling alternative to MBR processes, Desalination, 239 (2009) 10–21.
[16] C.R. Martinetti, A.E. Childress, T.Y. Cath, High recovery of concentrated RO brines using forward osmosis and membrane distillation, J. Membr. Sci., 331 (2009) 31–39.
[17] D. Rana, T. Matsuura, Surface modifications for antifouling membranes, Chem. Rev., 110 (2010) 2448–2471.
[18] X.Z. Zhao, J. Li, C.K. Liu, Improving the separation performance of the forward osmosis membrane based on the etched microstructure of the supporting layer, Desalination, 408 (2017) 102–109.
[19] X.Z. Zhao, C.K. Liu, Efficient removal of heavy metal ions based on the optimized dissolution-diffusion-flow forward osmosis process, Chem. Eng. J., 334 (2018) 1128–1134.
[20] N. Ma, J. Wei, R. Liao, C.Y. Tang, Zeolite-polyamide thin film nanocomposite membranes: towards enhanced performance for forward osmosis, J. Membr. Sci., 405–406 (2012) 149–157.
[21] K. Murata, K. Mitsuoka, T. Hirai, T. Walz, P. Agre, J.B. Heymann, A. Engel, Y. Fujiyoshi, Structural determinants of water permeation through aquaporin-1, Nature, 407 (2000) 599–605.
[22] A. Zirehpoura, A. Rahimpoura, M. Ulbricht, Nano-sized metal-organic framework to improve the structural properties and desalination performance of thin-film composite forward osmosis membrane, J. Membr. Sci., 531 (2017) 59–67.
[23] D.C. Ma, S.B. Peh, G. Han, S.B. Chen, Thin-film nanocomposite (TFN) membranes incorporated with super-hydrophilic metal-organic framework (MOF) UiO-66: toward enhancement of water flux and salt rejection, ACS Appl. Mater. Interfaces, 9 (2017) 7523–7534.
[24] W. Ding, J. Cai, Z. Yu, Q. Wang, Z. Xu, Z. Wang, C. Gao, Fabrication of an aquaporin-based forward osmosis membrane through covalent bonding of a lipid bilayer to a microporous support, J. Mater. Chem. A, 3 (2015) 20118–20126.
[25] L. Shen, J. Zuo, Y. Wang, Tris(2-aminoethyl)amine in-situ modified thin-film composite membranes for forward osmosis applications, J. Membr. Sci., 537 (2017) 186–201.
[26] W.P. Zhu, J. Gao, S.P. Sun, S. Zhang, T.S. Chung, Poly(amidoamine) dendrimer (PAMAM) grafted on thin-film composite (TFC) nanofiltration (NF) hollow fiber membranes for heavy metal removal, J. Membr. Sci., 487 (2015) 117–126.
[27] A.W. Bosman, H.M. Janssen, E.W. Meijer, About dendrimers: structure, physical properties, and applications, Chem. Rev., 99 (1999) 1665–1688.
[28] T.S. Chung, M.L. Chng, K.P. Pramoda, Y. Xiao, PAMAM dendrimer-induced cross-linking modification of polyimide membranes, Langmuir, 20 (2004) 2966–2969.
[29] G.L. Jadav, P.S. Singh, Synthesis of novel silica-polyamide nanocomposite membrane with enhanced properties, J. Membr. Sci., 328 (2009) 257–267.
[30] X.Z. Zhao, J. Li, C.K. Liu, A novel TFC-type FO membrane with inserted sublayer of carbon nanotube networks exhibiting the improved separation performance, Desalination, 413 (2017) 176–183.
[31] J. Yin, Y. Yang, Z. Hu, B. Deng, Attachment of silver nanoparticles (AgNPs) onto thin-film composite (TFC) membranes through covalent bonding to reduce membrane biofouling, J. Membr. Sci., 441 (2013) 73–82.
[32] Y.Q. Wang, X.Y. Li, C.L. Cheng, Y.B. He, J.F. Pan, T.W. Xu, Second interfacial polymerization on polyamide surface using aliphatic diamine with improved performance of TFC FO membranes, J. Membr. Sci., 498 (2016) 30–38.
[33] S.H. Park, Y.S. Ko, S.J. Park, J.S. Lee, J. Cho, K.Y. Baek, I.T. Kim, K. Woo, J.H. Lee, Immobilization of silver nanoparticle-decorated silica particles on polyamide thin-film composite membranes for antibacterial properties, J. Membr. Sci., 499 (2016) 80–91.
[34] X. Kong, Z.L. Qiu, C.E. Lin, Y.Z. Song, B.K. Zhu, L.P. Zhu, X.Z. Wei, High permselectivity hyperbranched polyester/polyamide ultrathin films with nanoscale heterogeneity, J. Mater. Chem. A, 5 (2017) 7876–7884.
[35] Y. Xiao, L. Shao, T.S. Chung, D.A. Schiraldi, Effects of thermal treatments, and dendrimers chemical structures on the properties of highly surface cross-linked polyimide films, Ind. Eng. Chem. Res., 44 (2005) 3059–3067.
[36] L. Shen, X. Zhang, J. Zuo, Y. Wang, Performance enhancement of TFC FO membranes with polyethyleneimine modification and post-treatment, J. Membr. Sci., 534 (2017) 46–58.
[37] C.K. Liu, R.B. Bai, Q.S. Ly, Selective removal of copper and lead ions by diethylenetriamine-functionalized adsorbent: behaviors and mechanisms, Water Res., 42 (2008) 1511–522.
[38] M.J. Ariza, J. Benavente, E. Rodriguez-Castellon, L. Palacio, Effect of hydration of polyamide membranes on the surface electrokinetic parameters: surface characterization by x-ray photoelectronic spectroscopy and atomic force microscopy, J. Colloid Interface Sci., 247 (2002) 149–158.
[39] M. Li, Z.W. Lv, J.F. Zheng, J.H. Hu, C. Jiang, M. Ueda, X. Zhang, L.J. Wang, Positively charged nanofiltration membrane with dendritic surface for toxic element removal, ACS Sustainable Chem. Eng., 5 (2017) 784–792.